

The following resources related to this article are available online at www.sciencemag.org (this information is current as of October 25, 2009):

Updated information and services, including high-resolution figures, can be found in the online version of this article at:

<http://www.sciencemag.org/cgi/content/full/325/5940/585>

Supporting Online Material can be found at:

<http://www.sciencemag.org/cgi/content/full/1173596/DC1>

A list of selected additional articles on the Science Web sites **related to this article** can be found at:

<http://www.sciencemag.org/cgi/content/full/325/5940/585#related-content>

This article **cites 37 articles**, 11 of which can be accessed for free:

<http://www.sciencemag.org/cgi/content/full/325/5940/585#otherarticles>

This article has been **cited by** 2 articles hosted by HighWire Press; see:

<http://www.sciencemag.org/cgi/content/full/325/5940/585#otherarticles>

This article appears in the following **subject collections**:

Neuroscience

<http://www.sciencemag.org/cgi/collection/neuroscience>

Information about obtaining **reprints** of this article or about obtaining **permission to reproduce this article** in whole or in part can be found at:

<http://www.sciencemag.org/about/permissions.dtl>

33. D. Ludwig, R. Hilborn, C. Walters, *Science* **260**, 17 (1993).
34. K. M. Brander, *Proc. Natl. Acad. Sci. U.S.A.* **104**, 19709 (2007).
35. P. A. Larkin, *Annu. Rev. Ecol. Syst.* **9**, 57 (1978).
36. A. A. Rosenberg, J. H. Swasey, M. Bowman, *Front. Ecol. Environ.* **4**, 303 (2006).
37. J. A. Hutchings, J. D. Reynolds, *Bioscience* **54**, 297 (2004).
38. U. R. Sumaila *et al.*, *Fish. Res.* **88**, 1 (2007).
39. J. Alder, U. R. Sumaila, *J. Environ. Dev.* **13**, 156 (2004).
40. J. S. Brashares *et al.*, *Science* **306**, 1180 (2004).
41. M. Dalton, S. Ralston, *Mar. Resour. Econ.* **18**, 67 (2004).
42. K. J. Sainsbury, R. A. Campbell, R. Lindholm, A. W. Whitelaw, in *Fisheries Management: Global Trends*, E. K. Pikitch, D. D. Huppert, M. P. Sissenwine, Eds. (American Fisheries Society, Bethesda, MD, 1997), pp. 107–112.
43. This work was conducted as part of the “Finding common ground in marine conservation and management” Working Group supported by the National Center for Ecological Analysis and Synthesis funded by NSF, the University of California, and the Santa Barbara campus. The authors acknowledge the Natural Sciences and Engineering Research Council (NSERC) and the Canadian Foundation for Innovation for funding database development, the Sea Around Us Project funded by

Pew Charitable Trusts for compiling global catch data, and numerous colleagues and institutions around the world for sharing fisheries assessment, catch, access, and survey data, and ecosystem models (see SOM for full acknowledgments).

Supporting Online Material

www.sciencemag.org/cgi/content/full/325/5940/578/DC1

Materials and Methods

Figs. S1 to S6

Tables S1 to S7

References and Notes

27 April 2009; accepted 22 June 2009

10.1126/science.1173146

Pre-Target Axon Sorting Establishes the Neural Map Topography

Takeshi Imai,^{1*} Takahiro Yamazaki,^{1*} Reiko Kobayakawa,¹ Ko Kobayakawa,¹ Takaya Abe,² Misao Suzuki,³ Hitoshi Sakano^{1†}

Sensory information detected by the peripheral nervous system is represented as a topographic map in the brain. It has long been thought that the topography of the map is determined by graded positional cues that are expressed by the target. Here, we analyzed the pre-target axon sorting for olfactory map formation in mice. In olfactory sensory neurons, an axon guidance receptor, Neuropilin-1, and its repulsive ligand, Semaphorin-3A, are expressed in a complementary manner. We found that expression levels of Neuropilin-1 determined both pre-target sorting and projection sites of axons. Olfactory sensory neuron-specific knockout of Semaphorin-3A perturbed axon sorting and altered the olfactory map topography. Thus, pre-target axon sorting plays an important role in establishing the topographic order based on the relative levels of guidance molecules expressed by axons.

In the vertebrate nervous system, sensory information is spatially encoded in the brain, forming topographic maps that are fundamental for cognition and higher-order processing of sensory information (1, 2). Molecular mechanisms of topographic map formation have been extensively studied in the visual system. The visual image on the retina is roughly preserved in the tectum, which receives retinal ganglion cell axons. Nearly 50 years ago, Sperry proposed the “chemoaffinity hypothesis,” in which target cells present chemical cues to guide axons to their destinations (3). Axonal projection of retinal ganglion cells is instructed by several pairs of axon guidance molecules that demonstrate graded expression in the retina and tectum (1, 2).

Olfactory information is also encoded in a topographic map formed on the olfactory bulb (OB), a part of the forebrain. In rodents, odors are detected with ~1000 types of odorant receptors (ORs) expressed in olfactory sensory neurons

(OSNs) in the olfactory epithelium (4). Each OSN expresses only one functional OR gene (5, 6). Furthermore, OSNs expressing a given type of OR converge their axons to a specific glomerulus on each glomerular map in the OB (7–9). During olfactory development, OSN axons are guided to approximate locations in the OB by the combination of dorsal-ventral patterning, based on anatomical locations of OSNs in the olfactory epithelium (10), and anterior-posterior patterning, regulated by OR-derived cyclic adenosine monophosphate (cAMP) signals (11, 12). The glomerular arrangement along the dorsal-ventral axis appears to be determined by axon guidance molecules expressed in a graded manner along the dorsomedial-ventrolateral axis in the olfactory epithelium, such as Robo-2 (13) and Neuropilin-2 (14). Unlike dorsal-ventral positioning, anterior-posterior positioning of glomeruli is independent of positional information in the olfactory epithelium. Instead, OR-specific cAMP signals determine the expression levels of Neuropilin-1 (Nrp1) in OSN axon termini, forming a gradient of Nrp1 (11). Thus, the olfactory system also uses gradients of axon guidance molecules to form the topographic map.

How then do guidance molecules regulate topographic map formation? Does map formation solely depend on axon-target interaction? Topographic order emerges in axon bundles, well before they reach the target (15, 16). Here, we studied the pre-target sorting of OSN axons and

its role in topographic map formation in the mouse olfactory system.

Nrp1 regulates axonal projection of OSNs along the anterior-posterior axis. OR-derived cAMP signals regulate the axonal projection of OSNs along the anterior-posterior axis in the OB; low cAMP leads to anterior positioning and high cAMP leads to posterior positioning (11). Furthermore, the levels of Nrp1 in OSN axon termini correlated with the level of cAMP signals (11).

We found that the Nrp1 levels determine the glomerular positioning along the anterior-posterior axis. When Nrp1 was overexpressed in OR-17-expressing OSNs (fig. S1), projection sites shifted posteriorly relative to the control (Fig. 1A and fig. S2). In contrast, when Nrp1 was knocked out specifically in I7 OSNs, the projection sites shifted anteriorly relative to the control (Fig. 1A and fig. S2). In the pan-OSN Nrp1 knockout, however, projection sites for I7 often split into anterior and posterior areas (fig. S3). If absolute Nrp1 levels determine glomerular positioning, all glomeruli should form in the anterior OB in the pan-OSN knockout, and the results for I7 OSNs should be the same between the I7-specific knockout and pan-OSN knockout. These results indicate that the relative Nrp1 levels among axons determine the OSN projection sites.

Pre-target axon sorting in the bundle. How do the relative levels of Nrp1 determine the anterior-posterior positioning of glomeruli in the axonal projection of OSNs? To determine where the organization occurs for the olfactory map topography, we analyzed the axon bundles of dorsal-zone (D-zone) OSNs that project to the dorsal domain (D domain) of the OB. The D domain OB comprises two regions, DI and DII; DI is represented by class I ORs, and DII is represented by class II ORs. Class I and class II ORs are phylogenetically distinct and their glomeruli are segregated in the OB (17). We subdivided DII into two areas on the basis of Nrp1 expression level (18): DII-P is the posterior portion innervated by Nrp1-high axons, and DII-A is the anterior region innervated by Nrp1-low axons. Thus, the D domain can be divided into three areas: DI, DII-A, and DII-P (Fig. 1B).

Axon bundles that project to the D-domain OB were analyzed in neonatal mice by staining serial coronal sections from the anterior olfactory epithelium through the OB. Within the bundle,

¹Department of Biophysics and Biochemistry, Graduate School of Science, University of Tokyo, Tokyo 113-0032, Japan.

²Laboratory for Animal Resources and Genetic Engineering, Center for Developmental Biology, RIKEN, Kobe 650-0047, Japan. ³Division of Transgenic Technology, Center for Animal Resources and Development, Kumamoto University, Kumamoto 860-0081, Japan.

*These authors contributed equally to this work.

†To whom correspondence should be addressed. E-mail: sakano@mail.ecc.u-tokyo.ac.jp

DI axons stained with DBA-lectin (fig. S4), DII-P axons stained with Nrp1 antibodies, and DII-A axons stained with neither. To visualize the Nrp1-low axon group (DII-A), we stained for yellow fluorescent protein (YFP)-positive OSNs that express the mutant OR gene *I7(RDY)-ires-gapYFP*; the I7(RDY) receptor is unable to activate downstream cAMP signals, thereby causing a lack of Nrp1 expression (11). Early in the trajectory of OSN projection, DI, DII-A, and DII-P axons were intermingled within the bundle. As the bundle progressed posteriorly, however, the axons segregated into a tripartite organization before they reached the target OB (Fig. 1B). Within the bundle, DI, DII-A, and DII-P axons were sorted to the medial, central, and lateral areas, respectively. Furthermore, there was a topographic order even within the DII-P axon group. Anterior-posterior positioning of glomeruli in the OB is well correlated with the central-lateral localiza-

tion of axons in the bundle (fig. S5). Thus, the olfactory map topography emerges within the axon bundle prior to the axon-target interactions in the OB.

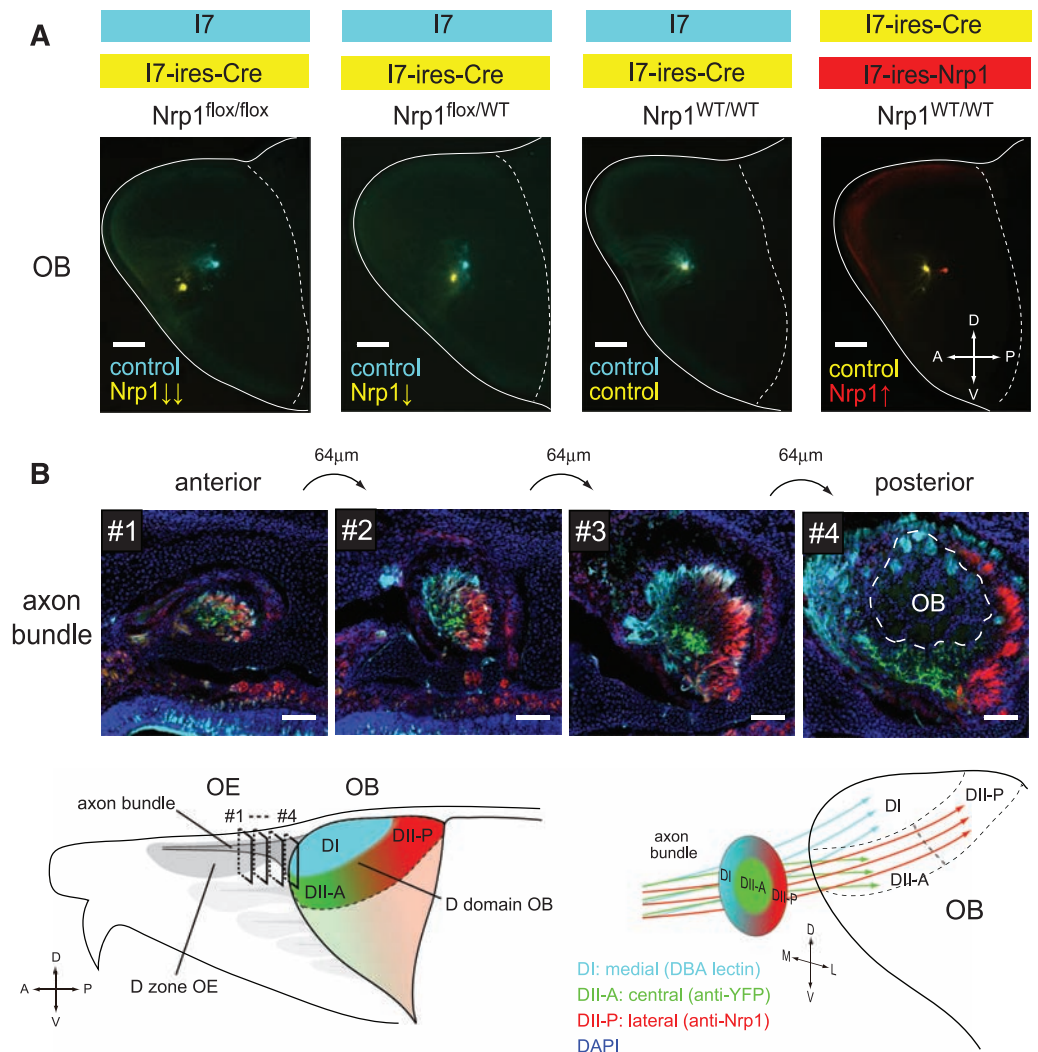
Heterotypic OSN axons segregate even without the OB (19, 20). We analyzed the *Gli3* mutant mouse (*Pdn/Pdn*), where the OB is completely absent, and found that the pre-target axon sorting indeed occurred (Fig. 2A) (21). In the *Pdn/Pdn* mutant, OSN axons demonstrated a graded anterior-posterior topography among the olfactory fibers in the cranial cavity (Fig. 2B), which supports the notion that the anterior-posterior topography can be formed, at least partially, without axon-target interactions.

Nrp1 regulates pre-target axon sorting. Because Nrp1-high (DII-P) and Nrp1-low (DII-A) axons are segregated within the bundles, we investigated whether Nrp1 is involved in the pre-target axon sorting. Wild-type I7 axons were normally

found among the Nrp1-positive DII-P axons in the lateral area in the bundle (Fig. 3A and fig. S6A). When Nrp1 was specifically knocked out in I7-expressing OSNs, these I7 axons moved to the central area (DII-A). In contrast to the wild-type I7, axons of the I7(RDY) mutant OSNs, which do not express Nrp1, were found in the central area (DII-A) of the bundle (Fig. 3B and fig. S6B). By simply expressing Nrp1 in these mutant OSNs with I7(RDY)-ires-Nrp1, axons moved to the lateral area (DII-P). Thus, Nrp1 indeed determines the sorting of DII-A (central) and DII-P (lateral) axons within the bundle.

Sema3A expressed by OSNs is required for axon sorting. Nrp1 is the receptor for the secreted repulsive ligand Semaphorin-3A (Sema3A) (22). Sema3A knockout disrupts proper targeting of OSNs (23, 24). We studied the possible involvement of Sema3A in pre-target axon sorting. *Sema3A* is expressed not only in the target, but also in OSNs. Single-cell microarray analysis revealed that *Nrp1*

Fig. 1. Projection and axon sorting of OSNs. (A) Genetic manipulation of Nrp1 expression levels in OSNs. Whole-mount fluorescent views of OBs (medial surface) were analyzed [age, postnatal day 14 (P14)]. For the loss of function of Nrp1, an I7-ires-Cre mouse (labeled with gap-YFP; yellow) was crossed to the floxed Nrp1 line. The projection site for the I7 (labeled with gap-CFP; cyan) was analyzed as an internal control in the same animal. In the $Nrp1^{fllox/fllox}$ background, Nrp1 was specifically knocked out in OSNs expressing I7-ires-Cre. As a result, projection sites were shifted anteriorly in the OB. In the $Nrp1^{fllox/WT}$ background, where the Nrp1 level was decreased by half, the anterior shifts were intermediate to those in the $Nrp1^{fllox/fllox}$ background. In the $Nrp1^{WT/WT}$ background, CFP- and YFP-labeled OSN axons coconverged. For the gain of function of Nrp1, we generated I7-ires-Nrp1 (labeled with gap-mCherry; red) and compared the projection site to that of the control construct, I7-ires-Cre. In the double transgenic mice, I7-ires-Nrp1 glomeruli were found posterior to the I7-ires-Cre glomeruli. Statistical data are in fig. S2. Scale bars, 500 μ m. **(B)** Pre-target axon sorting of OSNs. The axons of dorsal-zone (D-zone) OSNs course through the bundle on the dorsal roof of the olfactory epithelium before projecting to the D domain of the OB. The D domain comprises DI and DII domains in the OB. The DI domain is located in the most dorsal part of the OB; the DII domain is just ventral to DI and is further divided into DII-P (Nrp1-high; posterior) and DII-A (Nrp1-low; anterior). DI axons were stained with DBA lectin (cyan). DII-P axons were immunostained with antibodies to Nrp1 (red). For labeling of DII-A axons, OSN axons expressing I7(RDY)-ires-gapYFP were immunostained with antibodies to YFP (green). Three types of axons projecting to the DI, DII, and DII-P regions in the OB are intermingled in the bundle near the olfactory epithelium



but segregate to form a tripartite organization as they approach the OB. Coronal sections (#1 to #4, each separated by 64 μ m) are shown. DI, DII-A, and DII-P axons are sorted to the medial, central, and lateral areas, respectively. Scale bars, 100 μ m. OE, olfactory epithelium; A, anterior; P, posterior; D, dorsal; V, ventral; M, medial; L, lateral; ires, internal ribosome entry site.

Fig. 2. Anterior-posterior topography is established without the OB. The OB-less mutant *Pdn/Pdn* was analyzed. The *Pdn/Pdn* mouse has an insertional mutation within the *Gli3* gene coding for a transcription factor (21), resulting in agenesis of the OB. In the cranial cavity of these mutant mice, OSN axons form a fibrocellular mass (FCM). (A) Coronal sections of axon bundles from the wild-type and *Pdn/Pdn* mutant mice were analyzed (age, P0). OSN axons expressing I7(RDY)-ires-gapYFP were immunostained with antibodies to YFP. Axonal segregation occurred without the OB in the *Pdn/Pdn* mutant ($n = 6/6$). Scale bars, 100 μm . (B) Horizontal OB sections of the wild-type and mutant mice (age, P0) were immunostained with antibodies to Nrp1 (red) and gap43 (green); gap43 is an axonal marker for OSNs. In the glomerular layer of the wild-type OB, Nrp1 shows an anterior-low–posterior-high gradient (11). Similarly, in the mutant mouse (*Pdn/Pdn*), Nrp1 demonstrates an anterior-low–posterior-high gradient within the FCM in the absence of the OB. Nrp1 and gap43 immunoreactivities were quantified along the anterior-posterior axis of the FCM (along the dotted line). Mean signal intensities are normalized to 50. Data are means \pm SD ($n = 8$). OE, olfactory epithelium; Ctx, cerebral cortex. Scale bars, 500 μm .

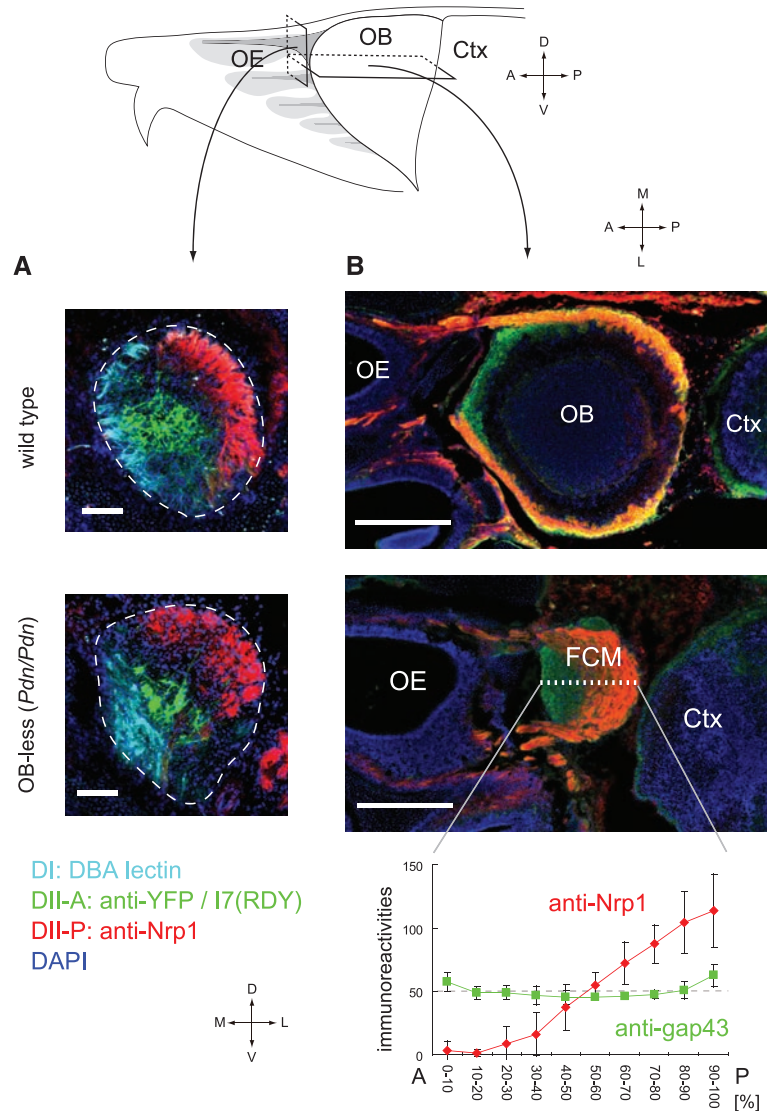
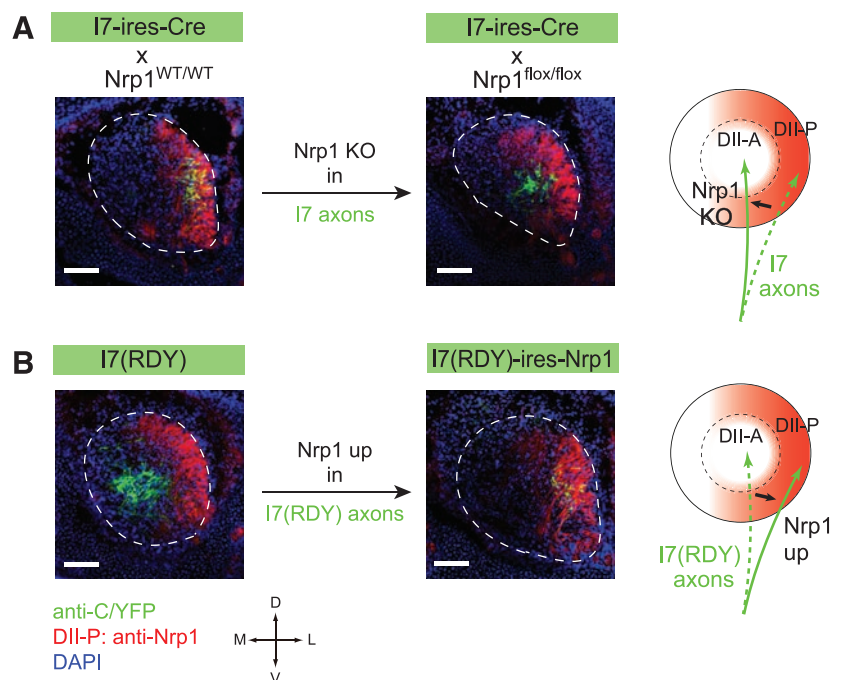


Fig. 3. Nrp1 regulates axon sorting in the bundle. (A) The loss-of-function experiment. Axons for I7-ires-Cre were sorted to the lateral peripheral area (DII-P). When Nrp1 was knocked out specifically in I7-ires-Cre OSNs, axons were sorted to the central region (DII-A). (B) The gain-of-function experiment. Axons for I7(RDY) that do not express Nrp1 were sorted to the central area of the bundle (DII-A). When Nrp1 was expressed specifically in I7(RDY) OSNs in the I7(RDY)-ires-Nrp1 mouse, axons were sorted to the lateral periphery (DII-P). Quantitative analyses are in fig. S6. Coronal sections of axon bundles (age, P0) were analyzed. Changes in axon sorting in the bundle are schematically shown at the right. Scale bars, 100 μm .



and *Sema3A* genes are regulated in a complementary manner by OR-derived cAMP signals (fig. S7) (25). In situ hybridization of embryonic olfactory epithelium demonstrated complementary expression of *Nrp1* and *Sema3A* (fig. S8A). To visualize the *Sema3A*-expressing OSN axons, we generated bacterial artificial chromosome (BAC) transgenic mice in which an axonal marker, *gap-YFP*, is expressed under the control of the *Sema3A* promoter (fig. S1). In the transgenic mouse, *Sema3A*-positive axons were found in the *Nrp1*-low area (DII-A) in the bundle (Fig. 4A and fig. S8B), which suggests that *Nrp1*-high axons (DII-P) are repelled by *Sema3A*-expressing axons (DII-A).

Because *Sema3A* is expressed in different cell types in olfactory tissues, we generated an OSN-specific knockout for *Sema3A* to investigate whether *Sema3A* in OSN axons is required for axon sorting within the bundle. We used the *OMACS* gene promoter, which is activated in the D-zone olfactory epithelium during early embryogenesis, to drive the expression of Cre recombinase (fig. S9) (26, 27). The *OMACS*-Cre mouse was crossed to the floxed *Sema3A* mouse (28) to generate the OSN-specific conditional knockout. In wild-type mice, *Nrp1*-positive DII-P axons are sorted to the lateral periphery of the bundle. In the conditional *Sema3A* knockout, however, the DII-P axons were no longer confined to the lateral periphery (Fig. 4A). Concomitantly, DII-A axons spread to more medial areas in the bundle. Tripartite compartmentalization was not evident in the OSN-specific *Sema3A* knockout. Thus, *Sema3A* derived from OSN axons is required for pre-target axon sorting in the bundle.

Pre-target axon sorting affects the topographic map formation in the OB. We asked whether perturbation of axon sorting mediated by OSN-derived *Sema3A* affects glomerular map formation in the OB. In wild-type mice, I7 axons that coexpress *gap-CFP* (cyan fluorescent protein) were sorted to the lateral-peripheral compartment (DII-P) within the bundle. In the conditional *Sema3A* knockout, however, I7 axons were found in the central area where the DII-A axons are normally found (Fig. 4B and fig. S10B). When I7 glomeruli were analyzed in the OB, anterior shifts were observed in the conditional knockout (Fig. 4B and fig. S11A), consistent with the shift of I7 axons in the bundle. We also analyzed *Nrp1*-negative DII-A axons in the conditional knockout (fig. S12). These axons were confined to the central area in the wild-type bundle. However, they were scattered to both the central and medial areas in the conditional knockout. As a result, glomeruli were found not only in the anterior but also in the dorsal OB in the conditional knockout. Thus, positional changes within the axon bundle correlate well with positional changes of glomeruli in the OB.

Discussion. We found that pre-target axon sorting plays an important role in the organization of the topographic map. *Nrp1* and its repulsive ligand *Sema3A* are both expressed in OSNs and are involved in axon sorting before targeting on the OB. Within the axon bundles

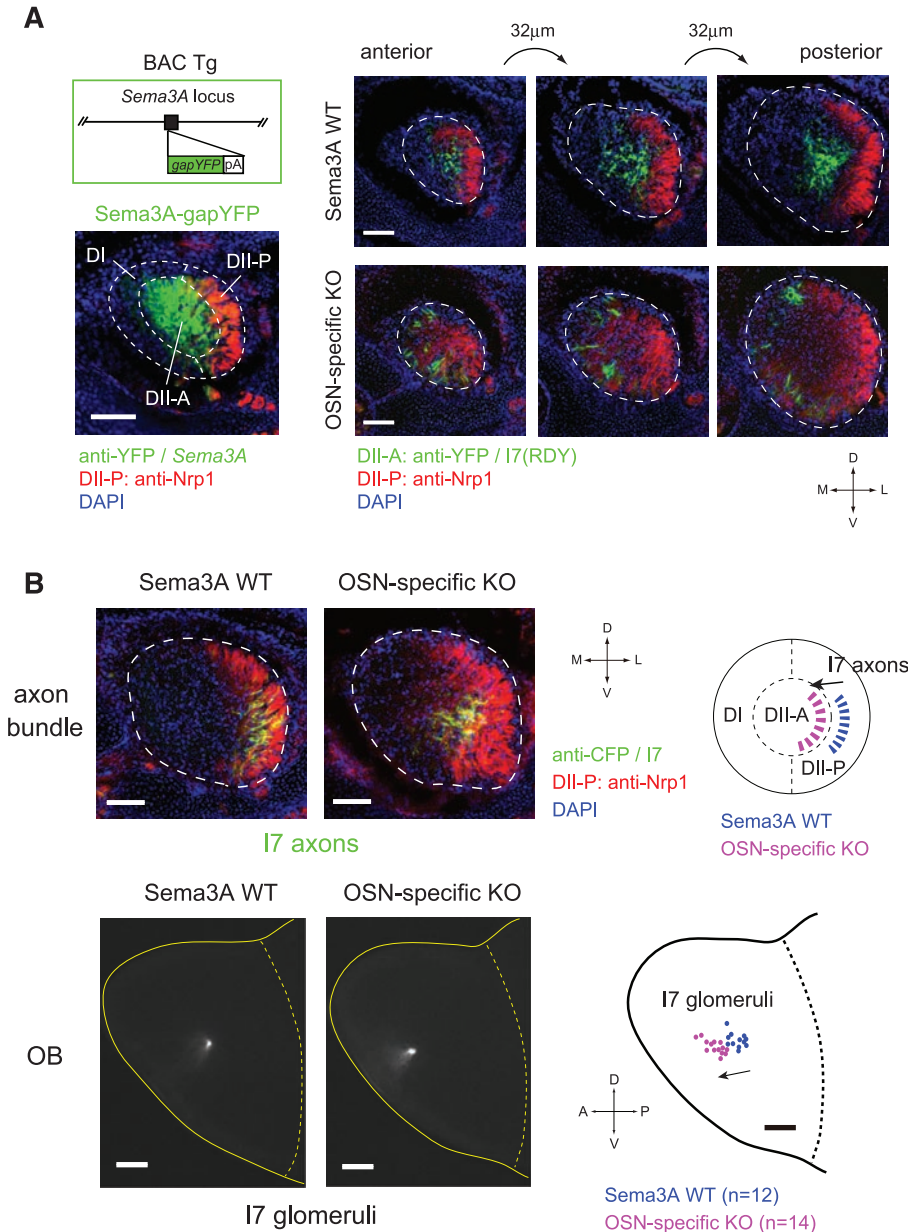


Fig. 4. OSN-derived *Sema3A* regulates not only pre-target axon sorting in the bundle, but also glomerular positioning in the OB. **(A)** Left panel: Segregation of *Nrp1*-expressing and *Sema3A*-expressing axons in the bundle (see also fig. S8B). The axonal marker protein *gap-YFP* was expressed under the *Sema3A* promoter in the BAC transgenic mice (age, P0). *Nrp1*-high DII-P axons were sorted to the lateral periphery (DII-P), whereas *Sema3A*-high axons were sorted to the central area (DII-A). Right panel: Axon sorting in the bundle in wild-type and OSN-specific *Sema3A* knockout mice. The conditional knockout mice were generated by crossing the *OMACS*-Cre line and the floxed *Sema3A* line (fig. S9). In the OSN-specific *Sema3A* knockout (age, P0), *Nrp1*-expressing axons (DII-P) spread out within the bundle, although they are still dense in the lateral region. I7(RDY) axons normally sorted to the central region (DII-A) are found in the medial region in the axon bundle. Scale bars, 100 µm. **(B)** Sorting and projection of I7-expressing OSN axons. In the wild-type mouse, I7 axons are sorted to the lateral periphery of the bundle. In contrast, in the OSN-specific *Sema3A* knockout, I7 axons are sorted to the central area, where DII-A axons are normally found (age, P0). Sorting patterns of I7 axons are schematically shown at the right (see also fig. S10B). Projection sites for I7 axons were analyzed in the OB (whole-mount medial views; age, P14). In the OSN-specific *Sema3A* knockout, I7 glomeruli were found anterior to the wild-type control. Results are summarized at the right; I7 glomeruli for the OSN-specific *Sema3A* knockout (14 bulbs, magenta) and wild-type littermates (12 bulbs, blue) are plotted on a schematic diagram of the medial OB (see also fig. S11A). Note that I7 OSN-specific *Sema3A* knockout did not affect the glomerular positioning (fig. S11B). Scale bars, 100 µm (axon bundles), 500 µm (OBs).

of D-zone OSNs, DII-A axons (Nrp1 low, *Sema3A* high) are sorted to the central compartment of the bundle, whereas DII-P axons (Nrp1 high, *Sema3A* low) are sorted to the lateral-peripheral compartment. This sorting appears to occur, at least in part, by the repulsive interaction between *Sema3A* and Nrp1. In addition to the repulsive interactions, *Sema3A* and Nrp1 signals may induce homophilic adhesion of axons with Nrp1 itself (29) or with other molecules such as L1 (30). Furthermore, additional guidance receptors such as Plexin-A1 (16) may be involved in the sorting of DII-A and DII-P axons (fig. S7). We assume that similar mechanisms are also at work in the sorting of DI and DII axons (Fig. 1B).

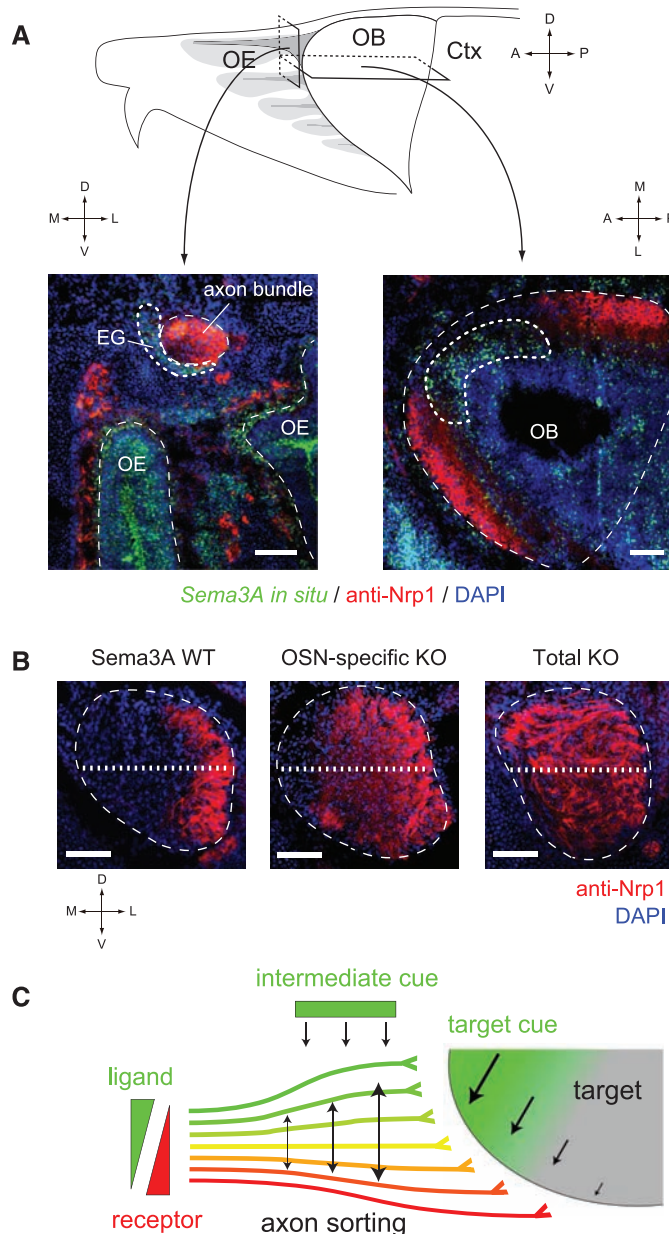
Once OSN axons are sorted in the bundle, they need to be oriented along the correct axis

before projecting onto a topographic map on the OB. This probably requires positional cues that are derived from the target or that are found along the pathway between the olfactory epithelium and the OB. In the *Sema3A* total knockout, Nrp1-positive DII-P axons spread rather uniformly across diameter of the bundle (Fig. 5B) and consequently mistarget to the anterior region in the OB (23, 24). The effect is different in the OSN-specific *Sema3A* knockout, where DII-P axons at least gravitate toward the lateral region in the bundle (Fig. 5B). Thus, *Sema3A* expressed by cells outside of the bundle likely functions as an additional guidance cue to orient the sorted axons along the correct axis for projection onto OB. In early embryos, but not in postnatal mice, *Sema3A* is expressed in the anterior OB (Fig. 5A). Fur-

thermore, *Sema3A* is found in ensheathing glial cells along the medial side of the axon bundles (Fig. 5A) (23). Involvement of such intermediate cues has been reported for the thalamocortical projection (31, 32).

In the *Drosophila* olfactory system, early-arriving OSN axons from the antenna repel late-arriving axons from the maxillary palp with *Sema1a* and Plexin-A, thereby segregating the two types of axons in the target (33). In the vertebrate retinotectal projection, target-derived guidance cues (e.g., ephrin-As) are thought to provide positional information. However, surgical and genetic studies indicated that projection sites for retinal ganglion cells are determined by relative, but not absolute, levels of guidance receptors, known as “axonal competition” (34, 35). Furthermore, retinal axons are presorted before the target recognition (15). Although retinal ephrin-As are thought to antagonize Eph-A receptors in cis (36), they may also function in trans to segregate heterotypic axons (37–39). We propose that the axon-axon interaction is a general strategy to establish the topographic order based on the relative levels of guidance molecules expressed by axons (Fig. 5C).

Fig. 5. *Sema3A* expressed by the non-OSN cells in the mouse olfactory system. (A) *Sema3A* mRNA is detected not only in OSNs, but also in the OB and ensheathing glia (EG) that surround axon bundles (age, E15). *Sema3A* expression is high on the medial side (Nrp1-low) of the axon bundle encircled by dotted line (left). In the OB, *Sema3A* is expressed in the anterior domain (encircled by dotted line) during early embryonic stages (right). Scale bars, 100 μ m. The mouse olfactory system (lateral view) is schematically shown at the top. (B) Coronal sections of axon bundles stained with antibodies to Nrp1 (age, P0). In the total knockout of *Sema3A*, Nrp1-positive axons are spread uniformly within the bundle (right). However, in the OSN-specific *Sema3A* knockout, Nrp1-positive axons gravitate to the lateral side of the bundle (middle). Thus, non-OSN *Sema3A* may help to orient the axon bundle organization. Quantification of Nrp1 immunoreactivities (along the dotted lines) is shown in fig. S10A. Scale bars, 100 μ m. (C) Possible mechanisms for topographic map formation in the brain. In the mouse olfactory system, a guidance receptor, Nrp1, and its repulsive ligand, *Sema3A*, are expressed in a complementary manner in OSNs. We propose that pre-target axon-axon interactions regulate the sorting of heterotypic axons. Target and intermediate cues may direct correct orientations of the map.



References and Notes

1. T. McLaughlin, D. D. O'Leary, *Annu. Rev. Neurosci.* **28**, 327 (2005).
2. L. Luo, J. G. Flanagan, *Neuron* **56**, 284 (2007).
3. R. W. Sperry, *Proc. Natl. Acad. Sci. U.S.A.* **50**, 703 (1963).
4. L. Buck, R. Axel, *Cell* **65**, 175 (1991).
5. B. Malnic, J. Hirono, T. Sato, L. B. Buck, *Cell* **96**, 713 (1999).
6. S. Serizawa *et al.*, *Science* **302**, 2088 (2003); published online 30 October 2003 (10.1126/science.1089122).
7. R. Vassar *et al.*, *Cell* **79**, 981 (1994).
8. K. J. Ressler, S. L. Sullivan, L. B. Buck, *Cell* **79**, 1245 (1994).
9. P. Mombaerts *et al.*, *Cell* **87**, 675 (1996).
10. K. Miyamichi, S. Serizawa, H. M. Kimura, H. Sakano, *J. Neurosci.* **25**, 3586 (2005).
11. T. Imai, M. Suzuki, H. Sakano, *Science* **314**, 657 (2006); published online 21 September 2006 (10.1126/science.1131794).
12. T. Imai, H. Sakano, *Curr. Opin. Neurobiol.* **17**, 507 (2007).
13. J. H. Cho, M. Lépine, W. Andrews, J. Parnavelas, J. F. Cloutier, *J. Neurosci.* **27**, 9094 (2007).
14. E. M. Norlin *et al.*, *Mol. Cell. Neurosci.* **18**, 283 (2001).
15. J. H. Scholes, *Nature* **278**, 620 (1979).
16. M. Satoda, S. Takagi, K. Ohta, T. Hirata, H. Fujisawa, *J. Neurosci.* **15**, 942 (1995).
17. A. Tsuboi, T. Miyazaki, T. Imai, H. Sakano, *Eur. J. Neurosci.* **23**, 1436 (2006).
18. H. Nagao, Y. Yoshihara, S. Mitsui, H. Fujisawa, K. Mori, *Neuroreport* **11**, 3023 (2000).
19. J. A. St John, H. J. Clarriss, S. McKeown, S. Royal, B. Key, *J. Comp. Neurol.* **464**, 131 (2003).
20. S. Yoshihara, K. Omichi, M. Yanazawa, K. Kitamura, Y. Yoshihara, *Development* **132**, 751 (2005).
21. I. Naruse, K. Kato, T. Asano, F. Suzuki, Y. Kameyama, *Brain Res. Dev. Brain Res.* **51**, 253 (1990).
22. T. S. Tran, A. L. Kolodkin, R. Bharadwaj, *Annu. Rev. Cell Dev. Biol.* **23**, 263 (2007).
23. G. A. Schwarting *et al.*, *J. Neurosci.* **20**, 7691 (2000).
24. M. Taniguchi *et al.*, *J. Neurosci.* **23**, 1390 (2003).
25. See supporting material on Science Online.
26. Y. Oka *et al.*, *Eur. J. Biochem.* **270**, 1995 (2003).
27. K. Kobayakawa *et al.*, *Nature* **450**, 503 (2007).
28. M. Taniguchi *et al.*, *Neuron* **19**, 519 (1997).
29. S. Takagi *et al.*, *Dev. Biol.* **170**, 207 (1995).

30. V. Castellani, A. Chédotal, M. Schachner, C. Favier-Sarrahil, G. Rougon, *Neuron* **27**, 237 (2000).
31. A. Dufour *et al.*, *Neuron* **39**, 453 (2003).
32. J. Seibt *et al.*, *Neuron* **39**, 439 (2003).
33. L. B. Sweeney *et al.*, *Neuron* **53**, 185 (2007).
34. M. G. Yoon, *J. Physiol.* **264**, 379 (1977).
35. A. Brown *et al.*, *Cell* **102**, 77 (2000).
36. M. R. Hornberger *et al.*, *Neuron* **22**, 731 (1999).
37. F. Bonhoeffer, J. Huf, *Nature* **315**, 409 (1985).
38. U. Drescher *et al.*, *Cell* **82**, 359 (1995).
39. B. W. Gallarda *et al.*, *Science* **320**, 233 (2008).
40. We thank D. D. Ginty and A. L. Kolodkin for Nrp1 mutant mice; M. Taniguchi and T. Yagi for Sema3A mutant mice; R. Y. Tsien for mCherry plasmid; and our laboratory members for valuable comments. Supported by the PREST program of the Japan Science and Technology Agency (R.K.), the Global COE program (K.K.), the Mitsubishi Foundation, and a Specially Promoted Research Grant from the Ministry of Education, Culture, Sports, Science and Technology of Japan.

Supporting Online Material

www.sciencemag.org/cgi/content/full/1173596/DC1
SOM Text
Figs. S1 to S12
References

16 March 2009; accepted 19 June 2009
Published online 9 July 2009;
10.1126/science.1173596
Include this information when citing this paper.

REPORTS

Grain Boundary Defect Elimination in a Zeolite Membrane by Rapid Thermal Processing

Jungkyu Choi,¹ Hae-Kwon Jeong,² Mark A. Snyder,³ Jared A. Stoeger,¹ Richard I. Masel,⁴ Michael Tsapatsis^{1*}

Microporous molecular sieve catalysts and adsorbents discriminate molecules on the basis of size and shape. Interest in molecular sieve films stems from their potential for energy-efficient membrane separations. However, grain boundary defects, formed in response to stresses induced by heat treatment, compromise their selectivity by creating nonselective transport pathways for permeating molecules. We show that rapid thermal processing can improve the separation performance of thick columnar films of a certain zeolite (silicalite-1) by eliminating grain boundary defects, possibly by strengthening grain bonding at the grain boundaries. This methodology enables the preparation of silicalite-1 membranes with high separation performance for aromatic and linear versus branched hydrocarbon isomers and holds promise for realizing high-throughput and scalable production of these zeolite membranes with improved energy efficiency.

Polycrystalline zeolite films (1–3) are used as membranes for alcohol dehydration (4) and are considered among other emerging technologies for various other high-resolution molecular separations (5). They have also been implemented in membrane reactors (6, 7) and used for a range of advanced applications (e.g., sensors, corrosion protection coatings, low-*k* dielectrics, and hosts for supramolecular organization of guest molecules) (8–11). A challenge stifling development and commercial realization of zeolite film technologies is the formation of cracks and/or grain boundary defects (12–14) during the thermal treatment required for removing structure-directing agents (SDAs) from zeolitic pores. Such defect structures are believed to degrade the separation performance of molecular sieve membranes by providing nonzeolitic and,

often, nonselective transport pathways for permeating species. Successful approaches to minimizing the effects of grain boundaries and cracks on membrane performance rely on microstructural optimization during film growth, including control of grain orientation and the formation of nanocomposites with the zeolite crystals embedded in the support pores (5, 15–18), as well as post-synthesis repair techniques (14, 19, 20). The complexity of these processes, however, hinders cost-effective and reliable scale-up of membrane production.

Heat treatment after hydrothermal film growth is a common technique for establishing accessible film microstructure. In this step, SDAs and/or other guest species occluded during crystal growth in the zeolite pores are removed. This calcination step is performed at very low heating rates in an attempt to minimize crack and other extra-zeolitic defect formation. Motivated by the persistence of defect structures despite such efforts to minimize their formation, we demonstrate the capabilities of rapid thermal processing (RTP) as a means for rapid microstructure development, substantial reduction of grain boundary defects, and marked improvements in membrane separation performance.

We demonstrate the influence of RTP on films of siliceous ZSM-5, also called silicalite-1.

Silicalite-1 is an all-silica zeolite with the MFI framework topology [(Si₉₆O₁₉₂)-MFI; for a description of MFI and other frameworks, see (21)]. MFI films are an excellent model system to investigate the effect of microstructure on film performance. Moreover, the ~6 Å pore opening of MFI enables separations of valuable components from commonly encountered chemical process streams like aromatic isomers and linear versus branched hydrocarbons. We focus on one class of siliceous MFI (hereafter referred to as MFI) films: *c*-out-of-plane-oriented films prepared by secondary growth of randomly oriented seeds (14, 22). These films and the associated synthesis techniques were chosen as a test-bed for evaluating the RTP approach based on the extensive previous characterization of film-growth mechanisms and separation performance. In addition, the high degree of film reproducibility and the versatility in film formation on various substrates makes this approach more amenable to scale up than other methods for synthesizing zeolite membranes.

The presence of transverse grain boundary defects produced during conventional (slow rate) calcination for SDA removal is well documented and has been correlated with poor separation performance (2, 13, 14, 23, 24). These grain boundary defects are formed in response to tensile stresses caused mainly by the abrupt zeolite unit cell contraction upon SDA removal, as well as by the mismatch of thermal expansion coefficients between the substrate and the zeolite film (13, 25). Depending on membrane operating conditions (temperature, pressure, mixture composition), the extrazeolitic pore openings at the grain boundaries may become substantially larger than the zeolite pores and, thus, compromise membrane performance (14). For example, the presence of grain boundary defects has been associated with the poor performance of *c*-oriented columnar membranes for xylene isomers (*p*- versus *o*-xylene) and the reduction of the mixture separation factor for butane isomers at elevated temperatures. For instance, despite the high single-component ideal selectivity (up to ~100) for xylene isomers, the separation factor for the corresponding binary mixture is less than 4 (14).

We explore the capabilities of RTP as the first heat treatment step after hydrothermal growth for reducing the formation of grain boundary

¹Department of Chemical Engineering and Materials Science, University of Minnesota, 151 Amundson Hall, 421 Washington Avenue SE, Minneapolis, MN 55455, USA. ²Artie McFerrin Department of Chemical Engineering, Texas A&M University, College Station, TX 77843–3122, USA. ³Department of Chemical Engineering, Lehigh University, 111 Research Drive, Bethlehem, PA 18015, USA. ⁴Department of Chemical and Biomolecular Engineering, University of Illinois at Urbana-Champaign, IL 61801, USA.

*To whom correspondence should be addressed. E-mail: tsapatsi@cems.umn.edu